



Return to isotropy of homogeneous shear-released turbulence

Ping-Fan Yang,¹ Alain Pumir ,^{2,3} and Haitao Xu ⁴

¹Center for Combustion Energy and Department of Energy and Power Engineering, Tsinghua University, 100084 Beijing, China

²Université Lyon, ENS de Lyon, Université Claude Bernard, Centre National de la Recherche Scientifique, Laboratoire de Physique, F-69342 Lyon, France

³Max Planck Institute for Dynamics and Self-Organization, 37077 Göttingen, Germany

⁴Center for Combustion Energy and School of Aerospace Engineering, Tsinghua University, 100084 Beijing, China



(Received 31 August 2020; accepted 17 March 2021; published 2 April 2021)

The presence of mean velocity gradients induces anisotropies in turbulent flows, which affect even the smallest scales of motion at finite Reynolds numbers. By performing direct numerical simulations of the Navier-Stokes equations, we study the return to isotropy of a homogeneous turbulent flow initially in a statistically stationary state under a uniform shear, $S = \frac{\partial U_1}{\partial x_2}$, in the conceptually simple situation where the mean shear is suddenly released. In particular, we characterize the timescales involved in the dynamics. We observe that the Reynolds stress tensor, which measures the large-scale flow anisotropy, relaxes towards an isotropic form over a timescale of the order of the large-eddy turnover time of turbulence, in qualitative agreement with previous studies with different types of initially imposed mean velocity gradient. We also investigate how the correlations of the velocity gradient tensor relax to isotropy with time. In particular, we focus on the properties of the one-point vorticity correlations $\langle \omega_i \omega_j \rangle$ and $\langle \omega_i \omega_j \omega_k \rangle$. The nonzero off-diagonal term of the second-order correlation tensor, i.e., the correlation between the streamwise and the transverse components of vorticity, $\langle \omega_1 \omega_2 \rangle$, decreases towards 0 over a time of the order of the Kolmogorov timescale. In comparison, the anisotropies in the diagonal components $\langle \omega_i^2 \rangle$ ($i = 1, 2, \text{ or } 3$) relax over a time significantly longer than the Kolmogorov timescale. This difference can be explained by an elementary theoretical analysis of the dynamics of the anisotropy tensor $b_{ij}^o \equiv \frac{\langle \omega_i \omega_j \rangle}{\langle \omega_k \omega_k \rangle} - \frac{1}{3} \delta_{ij}$ at the instant when the shear is released. We also observe that the skewness of the spanwise component of vorticity, S_{ω_3} , relaxes slowly towards zero. The relaxation of a small-scale quantity over a time much longer than the Kolmogorov timescale, as surprising as it may seem, is in fact consistent with a known relation between velocity-gradient correlations and the pressure-rate-of-strain correlation, and raises the important question of separation between the timescales characterizing the return to isotropy at large and small scales.

DOI: [10.1103/PhysRevFluids.6.044601](https://doi.org/10.1103/PhysRevFluids.6.044601)

I. INTRODUCTION

Whereas the paradigm of homogeneous, isotropic turbulence (HIT) provides a convenient frame to analyze flows at high Reynolds numbers [1–6], HIT can be realized only in numerical simulations

Published by the American Physical Society under the terms of the [Creative Commons Attribution 4.0 International](https://creativecommons.org/licenses/by/4.0/) license. Further distribution of this work must maintain attribution to the author(s) and the published article's title, journal citation, and DOI. Open access publication funded by the Max Planck Society.

or achieved approximately in specially designed experimental facilities, such as decaying grid turbulence in a wind tunnel. In practical situations, fluids are set into motion typically by inducing relative velocities, usually in a very anisotropic manner [7,8]. This is in particular the case of flows close to walls, which are subject to strong shear. In situations where the anisotropic forcing is localized, in space and/or in time, the turbulent fluctuations ultimately decay, and in so doing, they are expected to possess isotropic properties.

We focus here on the simplified problem of *homogeneous* anisotropic turbulence, more specifically, on its evolution when the imposed forcing is released. A convenient way to generate homogeneous anisotropic turbulence consists in applying a uniform velocity gradient to the flow. Flows subject to a pure strain, leading to either axisymmetric contraction or expansion, provide an important example, particularly relevant to flows through conduits of variable cross section in engineering devices [9–12]. Another well-studied example is the case of sheared turbulence. Early work has been devoted mostly to the development, in space [13–15] or in time [16–18] of sheared turbulence, including situations where the shear is released [19]. Interestingly, the properties of turbulence in the presence of a uniform shear in a confined system, when the flow reaches a statistically steady state, turn out to be relevant not only to the structure of the fine scales [20–28], but even to the description of the large scales of the motion [21,29–31]. In fact, the properties of homogeneous shear flows (HSFs) in a steady state even seem to provide useful insight on the structure, e.g., in the logarithmic layer of a turbulent channel flow [32]. Here we study the evolution of a homogeneous shear flow initially in a statistically stationary state followed by the turning off of the shear, which we denote as the homogeneous shear released turbulence (HSRT) following [19], and we investigate the degree of anisotropy in the large and small scales of the flow.

The Reynolds stress tensor, $\langle u_i u_j \rangle$, which equals $\frac{1}{3} \langle \mathbf{u}^2 \rangle \delta_{ij}$ in an isotropic flow, provides a very natural way to quantify the flow anisotropy. The Reynolds stress is sensitive to the largest scales of the flow, which are assumed to relax slowly towards isotropy after the imposed mean gradient is released. For a homogeneous flow in the absence of any forcing, the return of the Reynolds stress tensor towards the isotropic form is driven by the viscous dissipation and by the pressure-rate-of-strain correlation, $\langle ps_{ij} \rangle$ [33], where $s_{ij} \equiv (\partial_i u_j + \partial_j u_i)/2$ is the rate of strain tensor of the turbulent fluctuation and $\partial_i u_j$ denotes throughout the partial derivative $\partial u_j / \partial x_i$. Understanding these different terms is not only of fundamental interest; it has also important potential implications in engineering [8]. For lack of a complete understanding, modeling the return to isotropy rests on a simplifying assumption of linearity [34], with later improvements [35,36], all of which assume that the Reynolds stress evolves at the timescale corresponding to the largest eddies or the integral timescale of the flow; see [8] for a review.

The classical K41 theory hypothesizes that the degree of anisotropy of turbulent fluctuations decreases from large to small scales [1,8,37]. In the case of a turbulent HSF in a statistically stationary state, it is worth pointing out that the anisotropy induced by the shear decreases very slowly with scale [20,22,23,38], slower than anticipated based on phenomenological arguments [39,40]. For this reason, it is intrinsically interesting to ask how the sizable anisotropy present at all scales in a turbulent HSF at moderate Reynolds numbers decays when the shear is released. On general grounds, the small-scale anisotropies are expected to decay much faster than those affecting the largest scales of the flow. In particular, the anisotropy in the velocity gradient is expected to decay with the Kolmogorov timescale, the smallest timescale of the turbulence. It is, however, interesting to notice that the pressure-rate-of-strain correlation, $\langle ps_{ij} \rangle$, can be expressed as an integral over space of the triple correlation function of the velocity gradient tensor, $\tilde{T}_{abcdef}(\mathbf{x}) \equiv \langle \partial_a u_b(\mathbf{0}) \partial_c u_d(\mathbf{0}) \partial_e u_f(\mathbf{x}) \rangle$. A consequence of the relation between $\langle ps_{ij} \rangle$, which governs the decay of the Reynolds stress, and \tilde{T}_{abcdef} , a correlation function of the velocity derivatives, hence a small-scale quantity, is that the expectation that anisotropies related to the velocity gradient tensor should decay over a very fast timescale [12,36] should be considered with care. One of the main objectives of this work is to characterize the timescales involved in the relaxation of HSF towards isotropy after the shear is released.

To this end, we investigate by direct numerical simulation (DNS) the decay of the Reynolds stress tensor and the correlations of the velocity gradient tensor in homogeneous shear-released turbulent flows that are initially maintained at statistically steady states at moderate Reynolds numbers. Our results concerning the relaxation of the Reynolds stress tensor are generally consistent with earlier studies [36]: the relaxation to isotropy occurs over the integral timescale of the flow. We find, however, that the relaxation of the velocity gradient correlations towards isotropy cannot be simply reduced to a universal functional form by nondimensionalizing time by the Kolmogorov timescale. We rationalize our observations by studying the decay of the anisotropy in the vorticity correlation tensor, $\langle \omega_i \omega_j \rangle$, of which the different components decay with different characteristic timescales. Our analysis can be applied to other types of decaying anisotropic flows and the predictions of the decaying timescales for different components of velocity gradient tensors are consistent with the observations from DNS reported in the literature. We also discuss the relaxation of the pressure-rate-of-strain correlation function towards 0, its isotropic value.

Our paper is organized as follows. Section II briefly describes the numerical work carried out here. The dynamics of relaxation of the large scales of the flow towards isotropy is discussed in Sec. III. In Sec. IV we present our numerical results concerning the relaxation of the small scales towards isotropy. In particular, we compare our numerical results concerning the time evolution of the the vorticity correlation functions, $\langle \omega_i \omega_j \rangle$ and $\langle \omega_i \omega_j \omega_k \rangle$ with elementary analytic considerations, which provide insight about the timescales of the decay involved in different components. Finally, we summarize our results in Sec V.

II. DIRECT NUMERICAL SIMULATIONS

A. General approach

The present investigation is entirely based on DNS of the Navier-Stokes equations. We first simulated a turbulent homogeneous shear flow, by decomposing the turbulent velocity field \mathbf{U} , as the sum of a mean shear, $\langle \mathbf{U} \rangle = S x_2 \mathbf{e}_1$, where S is the shear rate, plus a fluctuation, \mathbf{u} . We used a pseudospectral code, assuming the fluctuation \mathbf{u} to be periodic in all three spatial directions, and homogeneous in space [41]. As demonstrated in earlier work [20,21], the flow reaches a statistically steady state in a finite box, albeit with important fluctuations at large scales.

After the flow has reached the statistically steady state, we merely released the shear rate to $S = 0$ and studied the subsequent evolution of the flow. Specifically, we studied the decay of turbulence from two runs at different Reynolds numbers. To address the variability induced by the large-scale fluctuations of the flow, for each initial Reynolds number, we accumulated statistics by simulating the decay of turbulence starting from a large number of different initial configurations. Throughout the paper, the angle brackets “ $\langle \rangle$ ” denote ensemble averages over different realizations and over space.

B. Simulations of homogeneous shear flow

We briefly discuss here the simulations of the flow in the presence of a mean shear. The code used here is based on the pseudospectral method introduced by Rogallo [41]. Our implementation has been described in [21]. We denote by x_1 , x_2 , and x_3 the coordinates in the streamwise, normal, and spanwise directions. As it was the case in [32,42], the homogeneous shear flow is simulated in a periodic domain of size $L_1 = 4\pi$ and $L_2 = L_3 = 2\pi$ using the method introduced in [41]. Numerically, we used a mesh with $2N \times N \times N$, with $N = 100$ and $N = 160$ for the two different runs. We adjusted the viscosity ν to keep the ratio between the mesh size, $\Delta x = 2\pi/N$ and the Kolmogorov length, $\eta_K = (\nu^3/\varepsilon)^{1/4}$, where ε is the rate of dissipation, to be approximately constant: $\Delta x/\eta_K \approx 2.2$, which ensures a satisfactory resolution of all scales of the flow. The values of the viscosity and the resolution, N , are indicated in Table I.

With the values chosen, the Reynolds number defined as $\text{Re} = SL_2^2/\nu$ reaches the values of $\text{Re} = 5.56 \times 10^3$ for the $N = 100$ case, and $\text{Re} = 1.04 \times 10^4$ for $N = 160$. To quantify the intensity of

TABLE I. Comparison between the moments and the skewnesses of components of the velocity gradient, and the Reynolds number of the homogeneous shear flow determined from the full simulations and from the N_c samples of configurations used as the starting point to study the restoration of isotropy. Columns 1 and 2 (respectively 3 and 4) correspond to the low (respectively high) Reynolds number run. The Reynolds number, Re , the duration of the runs, T_r , made dimensionless by multiplying by the shear, S , the viscosity, ν , and the resolution, N , are indicated in the upper part.

	$Re = 5.56 \times 10^3$ $ST_r = 1320$ $\nu = 7.1 \times 10^{-3}$	$Re = 5.56 \times 10^3$ $N_c = 41$ $N = 100$	$Re = 1.04 \times 10^4$ $ST_r = 734$ $\nu = 3.8 \times 10^{-3}$	$Re = 1.04 \times 10^4$ $N_c = 39$ $N = 160$
$\langle u_1 u_1 \rangle$	1.71	1.60	1.65	1.76
$\langle u_2 u_2 \rangle$	0.92	0.90	0.85	0.94
$\langle u_3 u_3 \rangle$	0.98	0.94	0.91	1.0
$\langle u_1 u_2 \rangle$	-0.53	-0.48	-0.49	-0.51
$\langle \omega_1 \omega_1 \rangle$	27.5	27.1	45.8	49.6
$\langle \omega_2 \omega_2 \rangle$	24.0	23.9	41.3	44.7
$\langle \omega_3 \omega_3 \rangle$	23.3	23.1	41.0	44.6
$\langle \omega_1 \omega_2 \rangle$	6.06	6.04	7.90	8.25
R_λ	113	107	155	160
$\langle (\partial_2 u_1)^2 \rangle$	10.9	10.8	18.2	19.8
$\langle (\partial_2 u_1)^3 \rangle$	26.6	26.5	51.2	57.5
$S_{\partial_2 u_1}$	0.74	0.75	0.66	0.65
$\langle \omega_3^2 \rangle$	-51.5	-50.7	-106.4	-121.6
S_{ω_3}	-0.46	-0.43	-0.41	-0.41

turbulence in a flow, it is customary to use the Taylor microscale-based Reynolds number [8]. Given the anisotropy of the flow, different definitions of the Taylor microscale-based Reynolds number are possible [43]. In this work, we use the definition that are traditionally measured using standard hot-wire anemometry, as done, e.g., in [22,23]:

$$R_\lambda = \frac{\langle u_1^2 \rangle^{1/2} \times \lambda}{\nu} \quad \text{with} \quad \lambda^2 = \frac{\langle u_1^2 \rangle}{\langle (\partial_1 u_1)^2 \rangle}, \quad (1)$$

where ∂_1 denotes $\partial/\partial x_1$. Using the values of $\langle u_1^2 \rangle$ and $\langle (\partial_1 u_1)^2 \rangle$ averaged over these runs, the Taylor microscale-based Reynolds numbers are found to be $R_\lambda = 113$ at the lower resolution and $R_\lambda = 155$ at the higher one. The corresponding values of R_λ are in the low range reached in the experiments [22,23], but are otherwise comparable with those obtained numerically in [30]. Another point of comparison is provided by simulations of turbulent channel flow. In a channel flow at $Re_\tau = 1000$ [44], the values of R_λ in the log layer are comparable to those of the present simulations, as discussed in [32]. Note that the values shown here slightly differ from those reported earlier in Ref. [42], which gave $R_\lambda = 120$ and $R_\lambda = 145$, respectively. The difference is partially due to the strong fluctuations in the instantaneous values of the spatial averages of u_1^2 and $(\partial_1 u_1)^2$, and partially to the longer duration of the run, T_r , used here, compared to that in [42]. With the current runs, we estimate the uncertainties for the values of R_λ to be approximately 3%.

For each Reynolds number, while integrating the equations of motion in the presence of a shear [32,42], a total of N_c ($N_c = 41$ for $R_\lambda = 113$ and $N_c = 39$ for $R_\lambda = 155$) configurations of the entire velocity fields were saved, all corresponding to the flow in the statistically stationary state, and well separated from each other in time. We used each of these configurations as the starting point of a new simulation with the mean shear released, as explained in the following subsection.

In the statistically steady state, one can define the following two timescales to characterize the fluid motion, namely, the Kolmogorov timescale, τ_η , and the large eddy turnover time, T_E , defined

by

$$\tau_\eta = \left(\frac{\nu^3}{\varepsilon}\right)^{1/4} \quad \text{and} \quad T_E = \frac{L_2}{\langle u_1^2 \rangle^{1/2}}, \quad (2)$$

where L_2 is the extent of the box in the normal direction, x_2 . The definition of τ_η corresponds to the definition used in an isotropic turbulent flow, but differs by no more than a few percents of any other definition using different components of velocity gradient or their combinations. The definition of T_E , however, is admittedly more arbitrary. The timescales defined by Eq. (2), and determined in the statistically stationary regime, will be used to characterize the dynamics after the shear is released.

C. Simulations of the flow after releasing the shear

Starting from the fluctuation \mathbf{u} of the turbulent homogeneous shear flow, we release the shear at a given time. As the solutions are still periodic in space, the evolution equation can be integrated in a straightforward manner with a standard pseudospectral code. We used here the code described in [45]. We kept the same viscosity and the same spatial resolution in our runs as in the calculations of sheared turbulence. We stress that the runs with and without shear differ in an essential way: whereas shear induces a spontaneous forcing mechanism [21], the runs are not forced after the shear is released, and decay in time. Each decaying run was integrated for a time corresponding to approximately one large-eddy-turnover timescale T_E defined by Eq. (2).

1. Statistical convergence

As the results presented after the shear is released rest on averaging over an ensemble of simulations each with a different starting point, it is important to provide an estimate of the statistical uncertainties. To evaluate the quality of the statistics obtained from the N_c configurations, we compared some lower-order moments of the homogeneous shear flow obtained by averaging over the entire time of the run, and from the N_c selected configurations, for each of the two Reynolds numbers investigated. As shown in Table I, the Reynolds stress tensor, $\langle u_i u_j \rangle$, as well as the second moments of the vorticity components, $\langle \omega_i \omega_j \rangle$ determined from the entire run and from the N_c configurations differ by less than $\sim 10\%$. Table I also shows the third moments of $\partial_2 u_1$ and of ω_3 , which provide a measure of the anisotropy of the homogeneous turbulent shear flow. The corresponding estimates of the skewness of these two quantities differ by less than $\sim 7\%$. With the values shown in Table I, the value of the large-eddy-turnover time is $T_E \approx 4.8 S^{-1}$.

In addition, we have evaluated separately the sample to sample fluctuations of the various moments computed from different configurations, and we found the fluctuations to be consistent with the 10% differences shown in Table I. For the Reynolds number, the values of R_λ obtained from individual configurations differ by less than $\sim 3.5\%$.

III. RETURN TO ISOTROPY: LARGE-SCALE PROPERTIES

In this section, we discuss the return of the flow to isotropy from the point of view of the turbulence properties at large scales characterized by the Reynolds stress tensor $\langle u_i u_j \rangle$. As was done for other flows (see, e.g., [12,36,46,47]), we introduce the anisotropy tensor, \mathbf{b} , defined by

$$b_{ij} \equiv \frac{\langle u_i u_j \rangle}{\langle u_k u_k \rangle} - \frac{1}{3} \delta_{ij}. \quad (3)$$

Figure 1(a) shows the evolution of the nonzero components of the tensor \mathbf{b} with time, for the two Reynolds numbers. Time has been normalized by the corresponding large-eddy turnover time T_E , defined by (2). The evolution of the tensor \mathbf{b} at the two Reynolds numbers with t/T_E is very close to each other, which indicates that the properties of the decaying turbulent shear flow, as described by the Reynolds stress tensor or equivalently by the tensor \mathbf{b} , return to isotropy over a characteristic time T_E .

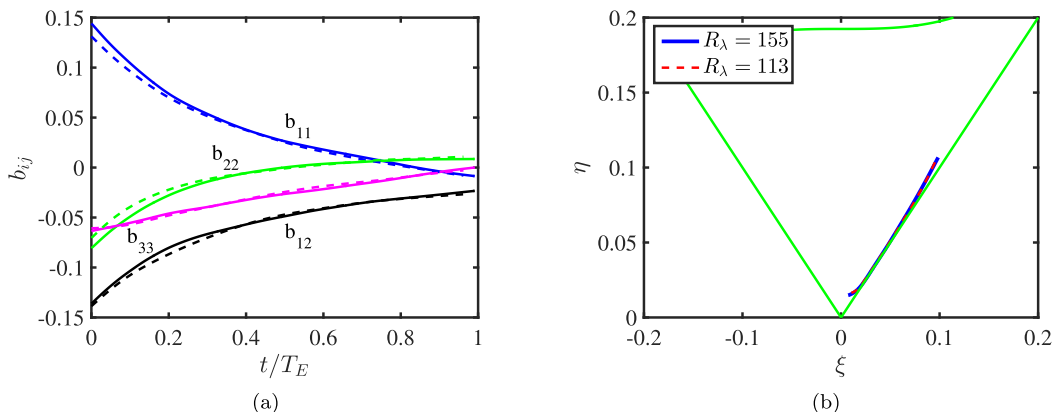


FIG. 1. (a) Evolution of components of the Reynolds stress anisotropy tensor b_{ij} . (b) Trajectories of the return to isotropy of HSRT on the ξ - η invariant map. The green lines delineate the Lumley triangle. In both plots, the full lines correspond to $R_\lambda = 155$ and the dashed lines to $R_\lambda = 113$. The trajectories of the two Reynolds numbers on the Lumley triangle essentially superpose.

By construction, the tensor \mathbf{b} is traceless and symmetric. As a result, aside from an overall rotation, it can be fully characterized by two extra quantities. We use here the two sets of invariants ξ and η , or II and III defined in [8] as

$$6\eta^2 = b_{ij}b_{ji}, \quad \text{II} = -3\eta^2, \quad (4)$$

$$6\xi^3 = b_{ij}b_{jk}b_{ki}, \quad \text{III} = 2\xi^3. \quad (5)$$

The Reynolds stress tensor at any instant can be represented by a point on a plane defined by its corresponding invariants ξ and η , or II and III, and the points of all realizable turbulent flows are confined inside the area called the Lumley triangle [8,48]. When the flow is isotropic, $\mathbf{b} = \mathbf{0}$, all the invariants ξ , η , II and III are zero. The return of the flow toward isotropy can therefore be represented by a trajectory of the invariants ξ and η (or equivalently II and III) towards the origin in the corresponding plane. Figure 1(b) shows the trajectories describing the return to isotropy in the (ξ, η) plane for the two Reynolds numbers studied here. Despite the differences visible in Fig. 1(a), the two trajectories are very close to each other, implying at most a very weak dependence on the Reynolds number. The trajectories are not exactly straight lines: they first move closer to the right boundary of the Lumley triangle, $\xi = \eta$, which physically corresponds to axisymmetric turbulence with one large eigenvalue. This is consistent with previous observation [36,49] that turbulence tends to become axisymmetric while relaxing to an isotropic state. Interestingly, as one moves away from the wall towards the center in a turbulent channel flow, the relaxation towards isotropy of \mathbf{b} also occurs along the right side of the Lumley triangle; see Fig. 11.1 of [8].

For decaying homogeneous turbulence, the evolution equation for the Reynolds stress tensor, derived from the Navier-Stokes equations, reads

$$\frac{d}{dt} \langle u_i u_j \rangle = R_{ij} - \varepsilon_{ij}, \quad (6)$$

where the quantities on the right-hand-side (r.h.s.) of Eq. (6), ε_{ij} , the dissipation tensor, and R_{ij} , the pressure-rate-of-strain correlation tensor, are defined as

$$\varepsilon_{ij} \equiv 2\nu \left\langle \frac{\partial u_i}{\partial x_k} \frac{\partial u_j}{\partial x_k} \right\rangle \quad (7)$$

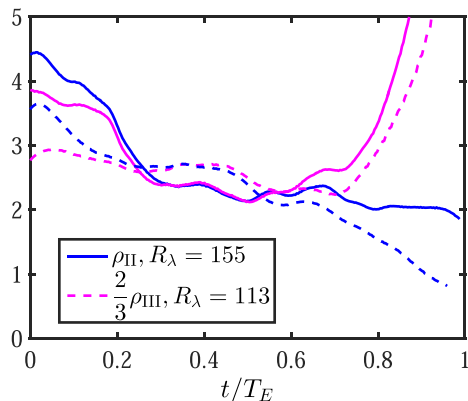


FIG. 2. Time dependence of the rates of return to isotropy of the invariants II and III. The blue lines correspond to $\rho_{\text{II}} = -\frac{E/\varepsilon}{\text{II}} \frac{d\text{II}}{dt}$ and the magenta lines to $\rho_{\text{III}} = -\frac{E/\varepsilon}{\text{III}} \frac{d\text{III}}{dt}$. The solid and dashed lines correspond to $R_\lambda = 155$ and $R_\lambda = 113$, respectively.

and

$$R_{ij} \equiv \frac{2}{\rho} \langle ps_{ij} \rangle. \quad (8)$$

Simple approximations are often used to model the evolution of the Reynolds stress tensor, in the spirit originally proposed by Rotta [34]:

$$\frac{d}{dt} \langle u_i u_j \rangle = \varepsilon \left[-2C_R b_{ij} - \frac{2}{3} \delta_{ij} \right], \quad (9)$$

where $\varepsilon = 2\nu \langle s_{ij} s_{ij} \rangle = \frac{1}{2} \varepsilon_{ii}$ is the turbulent energy dissipation rate. This parametrization implicitly assumes that the relaxation process is controlled by a single relaxation timescale, $\propto T_E$. The Rotta model, Eq. (9), predicts that the trajectory in the (ξ, η) plane is simply a straight line, connecting the initial value $(\xi(0), \eta(0))$ to the isotropic value $(0,0)$. As shown in Fig. 1(b), predictions of this simple model are at odds with the DNS data, as also observed previously [36,49]. The deviations of the trajectories from the straight-line representation on the (ξ, η) plane, shown in Fig. 1(b), can be better seen by studying the decay rates of the invariants II and III, defined as

$$\rho_{\text{II}} = -\frac{E/\varepsilon}{\text{II}} \frac{d\text{II}}{dt} \quad \text{and} \quad \rho_{\text{III}} = -\frac{E/\varepsilon}{\text{III}} \frac{d\text{III}}{dt}, \quad (10)$$

where $E \equiv \langle u_i u_i \rangle / 2$ is the turbulent kinetic energy. For these quantities, the Rotta model predicts that ρ_{II} and ρ_{III} are constant values with the relation $\rho_{\text{II}} = \frac{2}{3} \rho_{\text{III}}$ [cf. Eq. (11.37) in Ref. [8]].

Figure 2 shows the evolution in time of ρ_{II} and $\frac{2}{3} \rho_{\text{III}}$ from the DNS data. During the time interval $t/T_E \lesssim 0.6$, the values of ρ_{II} and $\frac{2}{3} \rho_{\text{III}}$ vary: they are larger at earlier time and later gradually decay, by approximately a factor of 2, which means a faster rate of return to isotropy at the beginning. This can be related to the evolution of the nonzero components of b_{ij} , shown in Fig. 1(a). Namely, although the absolute value of b_{33} , the anisotropy corresponding to the spanwise velocity component, starts out smaller than any of that of the three other nonzero components of \mathbf{b} , it relaxes over a significantly longer timescale. This is qualitatively consistent with a slower decay rate at $t/T_E \gtrsim 0.25$, hence a lower value of ρ_{II} and ρ_{III} , as shown in Fig. 2. At later times, $t/T_E > 0.6$, the value of ρ_{III} seems to increase rapidly. As a caveat, we observe that the determination of ρ_{II} and ρ_{III} becomes delicate for $t/T_E \gtrsim 0.6$, as the statistical uncertainties are playing an essential role when the tensor \mathbf{b} itself is small. More realizations would be necessary to confirm the tendency observed

in Fig. 2 at later times. Nevertheless, we notice that the trend is clearly visible at both Reynolds numbers, and that a similar observation has been reported before in previous numerical simulations of decaying anisotropic turbulence [46].

Most previous studies of the return to isotropy are for axisymmetric turbulent flows. It is instructive to compare the relaxation rate towards isotropy of the shear-released flow with other axisymmetric flows. Flows involving an axisymmetric expansion (AXE), corresponding to a positive value of the invariant III, and represented by a point close to the right boundary of the Lumley triangle in the (II, III) plane, are reported to return slower towards isotropy than flows involving an axisymmetric contraction (AXC), with III < 0 [36,47]. Specifically, the values of ρ_{II} in previous examples of AXE were found to be close to 0.5. For the HSRT studied here, the invariants III are also positive, and the Reynolds stress states also lie on the right side of the Lumley triangle, but with significantly larger values of $\rho_{II} \approx 2$, indicating a much faster return towards isotropy. In fact, the values of ρ_{II} for HSRT are comparable to those observed in AXC, with III < 0 and Reynolds stress invariants close to the left side of the Lumley triangle [36,47]. This observation points to a lack of universality of the return to isotropy, which is not very surprising when considering a large-scale quantity, such as the Reynolds stress tensor. A finer understanding of the physical processes is necessary to accurately describe the return of the flow towards isotropy.

In terms of modeling, we notice that the existence of significantly different timescales, implied by Figs. 1(a) and 2, cannot be simply captured by the nonlinear generalization of the relaxation model proposed in [50]. The initial phase of decay of the large-scale anisotropy is possibly related to a fast adjustment of the flow structure towards some universal anisotropic structure that then relaxes at a slower rate towards isotropy and might be treated by small perturbations of the isotropic turbulence. We speculate that the first stage is flow dependent, whereas the second phase corresponds to the numerically observed slower decay and could be captured by models that rely on the Reynolds stress tensor alone. These two distinct dynamical phases have been observed also in other anisotropic turbulent flows [46,47], as well as in decaying isotropic turbulence [51].

The suggestion that the relaxation to isotropy involves more than one timescale is an invitation to discuss more precisely the two terms involved in the evolution equation of the Reynolds stress tensor, Eq. (6). The dissipation tensor, ε_{ij} , defined by Eq. (7), involves only velocity derivatives and is therefore often assumed to return to isotropy very fast [12,36]. The pressure-rate-of-strain correlation tensor, R_{ij} , defined by Eq. (8), is often attributed to the large-scale properties of the flow, and therefore assumed to vary on a longer timescale $\sim T_E$. It is useful to recall in this context that pressure can be expressed as a solution of the Poisson equation: $\nabla^2 p(\mathbf{x}) = -\rho \partial_i u_j \partial_j u_i$. Considering the idealized case of a flow without boundary, this leads to the explicit expression for R_{ij} in terms of the third-order correlation of the velocity gradient tensor [8]:

$$R_{ij} = \frac{1}{4\pi} \int \frac{d\mathbf{x}'}{|\mathbf{x}'|} \langle \partial_k u_l(\mathbf{x}') \partial_l u_k(\mathbf{x}') (\partial_i u_j + \partial_j u_i)(\mathbf{0}) \rangle, \quad (11)$$

which means that the decay towards $\mathbf{0}$ of the anisotropic tensor \mathbf{b} , which depends on the large-scale flow property, is governed by a quantity that depends explicitly on the flow anisotropy at the smallest scales, namely, the third-order correlation of the velocity gradients. This casts doubt on the oversimplifying argument, according to which the smallest scales of the flow relax towards isotropy over the smallest flow timescale (the Kolmogorov time τ_η). We will revisit these aspects in Sec. IV.

IV. RETURN TO ISOTROPY: SMALL-SCALE PROPERTIES

A. Return of vorticity and dissipation towards isotropy

A straightforward way to extend the discussion of the relaxation to isotropy at large scale in Sec. III to the relaxation to isotropy at smaller scales consists in considering instead of the velocity

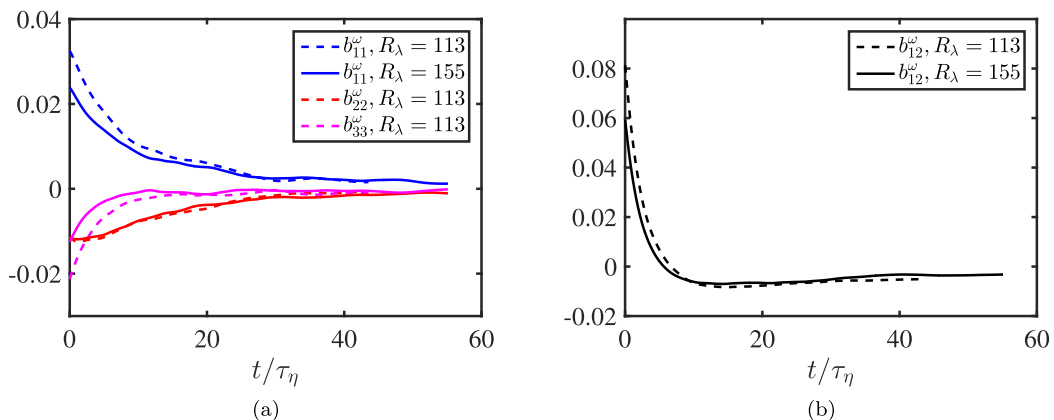


FIG. 3. Evolution of the components of the anisotropy tensor b_{ij}^ω , as a function of t/τ_η . (a) diagonal components b_{ii}^ω for $i = 1$ (blue), 2 (red), and 3 (magenta); (b) the nonzero off-diagonal component b_{12}^ω . The full lines represent the solution at $R_\lambda = 155$ and the dashed lines at $R_\lambda = 113$.

fluctuations the vorticity components, ω_i , and to define a tensor \mathbf{b}^ω by

$$b_{ij}^\omega = \frac{\langle \omega_i \omega_j \rangle}{\langle \omega^2 \rangle} - \frac{1}{3} \delta_{ij}. \quad (12)$$

Whereas the trace of $\langle \omega_i \omega_j \rangle$ is known to decay over a slow timescale $\sim T_E$, the relaxation of the tensor \mathbf{b}^ω is often postulated to occur over a fast timescale [12,36]. One of the reasons to focus on \mathbf{b}^ω is that it can be analyzed with the help of the analytic considerations presented in Sec. IV C. In the presence of a mean shear, symmetry imposes that only the diagonal components of b_{ij}^ω , and one off-diagonal term b_{12}^ω , are nonzero.

Figure 3 shows the evolution of the tensor b_{ij}^ω as a function of time for the two runs. The diagonal components b_{11}^ω , b_{22}^ω , and b_{33}^ω [see Fig. 3(a)] are shown separately from the only nonzero off-diagonal component b_{12}^ω [see Fig. 3(b)]. We begin by noticing that in Fig. 3 the values of b_{ij}^ω are much smaller than those of b_{ij} , almost by an order of magnitude. This is a consequence of the restoration of isotropy at small scales, so ω is not so much affected by the large-scale anisotropy induced by the mean shear. In Fig. 3 time is made dimensionless by τ_η . The off-diagonal component b_{12}^ω crosses 0 at $\sim 4\tau_\eta$ and overshoots slightly before returning slowly to 0. In comparison, the diagonal components of \mathbf{b}^ω decay monotonically towards 0, on a timescale that is $\gtrsim 10 \times \tau_\eta$ or on the order of T_E over the range of Reynolds number studied here, i.e., slower than the fast relaxation observed for b_{12}^ω at very short timescales. The behavior of b_{ij}^ω therefore suggests that the dynamics of small-scale quantities involve more than one timescale.

In the case of turbulent shear flows, the anisotropy at the smallest scales also manifests itself by the third moment of the fluctuation of the velocity gradient, $\partial_2 u_1$, and of the spanwise component of vorticity, ω_3 [20,32]. The corresponding skewnesses: $S_{\partial_2 u_1} \equiv \langle (\partial_2 u_1)^3 \rangle / \langle (\partial_2 u_1)^2 \rangle^{3/2}$ and $S_{\omega_3} \equiv \langle \omega_3^3 \rangle / \langle \omega_3^2 \rangle^{3/2}$ are of order 1 and decrease slowly with R_λ , as $\sim R_\lambda^{-0.5}$ [23]. The values of $S_{\partial_2 u_1}$ and S_{ω_3} are indicated in Table I. The time dependence of the skewnesses of $\partial_2 u_1$ and ω_3 is shown in Fig. 4. The dashed and full blue lines indicate $S_{\partial_2 u_1}$, at $R_\lambda = 113$ and 155, whereas the dashed and full magenta lines show $-S_{\omega_3}$, respectively, at $R_\lambda = 113$ and 155. Time is made dimensionless by the large eddy-turnover time, T_E . The relaxation of both $S_{\partial_2 u_1}$ and $-S_{\omega_3}$ occurs over a time of order T_E , although the limited range of Reynolds numbers covered by the present study prevents us from drawing a strong conclusion about the relaxation timescale. On the other hand, the evolutions of $S_{\partial_2 u_1}$ and $-S_{\omega_3}$ at the initial stage, i.e., for $\tau/\tau_\eta \sim O(1)$, also differ, consistent with earlier observations of the different behavior of the components of ε_{ij} and $\langle \omega_i \omega_j \rangle$.

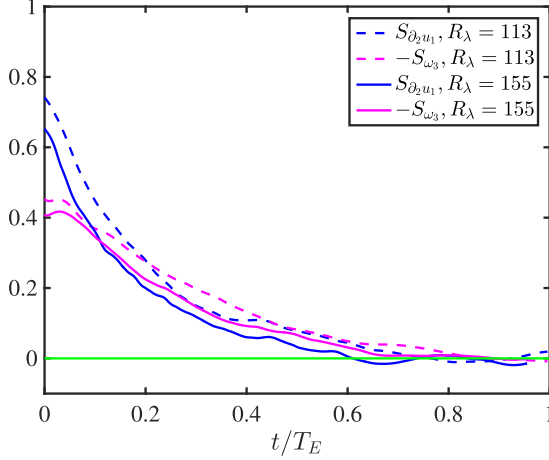


FIG. 4. Evolution of the skewness of $\partial_2 u_1$, $S_{\partial_2 u_1}$ (blue) and of ω_3 , S_{ω_3} (magenta). The full lines correspond to $R_\lambda = 155$ and the dashed lines to $R_\lambda = 113$.

To study the return to isotropy of the small scales, it is interesting to also consider the evolution of ε_{ij} , which is discussed in Appendix A.

B. Return to isotropy of the velocity gradient tensor

In the previous section, we presented numerical results on the decay of anisotropy, characterized by several small-scale quantities related to vorticity and dissipation. We now characterize the return to isotropy using the systematic characterization proposed in [42]. Namely, we introduce the second- and third-order velocity gradient correlation tensors:

$$\overline{T}_{abcd}^{2,\text{flow}} = \langle \partial_a u_b \partial_c u_d \rangle \quad \text{and} \quad \overline{T}_{abcdef}^{3,\text{flow}} = \langle \partial_a u_b \partial_c u_d \partial_e u_f \rangle, \quad (13)$$

which depend on the particular flow considered, as indicated by the superscripts. For homogeneous isotropic turbulence (HIT), both $\overline{\mathbf{T}}^{2,HIT}$ and $\overline{\mathbf{T}}^{3,HIT}$ depend on one scalar only, i.e.,

$$\overline{T}_{abcd}^{2,HIT} = \langle \partial_a u_b \partial_a u_b \rangle T_{abcd}^{2,HIT} \quad \text{and} \quad \overline{T}_{abcdef}^{3,HIT} = \langle \text{tr}(\mathbf{s}^3) \rangle T_{abcdef}^{3,HIT}, \quad (14)$$

where $\text{tr}(\mathbf{s}^3) = s_{ij}s_{jk}s_{ki}$. The explicit forms of $\mathbf{T}^{2,HIT}$ and $\mathbf{T}^{3,HIT}$ involve only the identity tensor δ_{ij} , the permutation tensor ϵ_{ijk} , and numerical factors [42]. For any turbulent flow, we consider the dimensionless form of the tensors $\overline{\mathbf{T}}^{2,\text{flow}}$ and $\overline{\mathbf{T}}^{3,\text{flow}}$ by defining

$$\mathbf{T}^{2,\text{flow}} = \frac{\overline{\mathbf{T}}^{2,\text{flow}}}{\langle \partial_a u_b \partial_a u_b \rangle} \quad \text{and} \quad \mathbf{T}^{3,\text{flow}} = \frac{\overline{\mathbf{T}}^{3,\text{flow}}}{\langle \text{tr}(\mathbf{s}^3) \rangle}. \quad (15)$$

The expressions for $\mathbf{T}^{n,\text{flow}}$ can be directly compared to $\mathbf{T}^{n,HIT}$, thus providing an explicit way to measure the anisotropy of the flow as measured by the second- and third-order moments of the velocity derivatives. To this end, we write

$$\mathbf{T}^{n,\text{flow}} = \zeta \mathbf{T}^{n,HIT} + \Theta^{n,\text{flow}}, \quad (16)$$

where the tensor Θ is taken as the deviation with respect to isotropy. Both the scalar coefficient ζ and the tensor Θ are obtained by minimizing the norm of $\|\mathbf{T}^{n,\text{flow}} - \zeta \mathbf{T}^{n,HIT}\|$.

To proceed, we use the following elementary symmetry considerations. In the case of HIT, all the components of the tensor with an odd number of any of 1, 2, and 3 among the indices are zero. In the homogeneous shear flow (HSF) considered here, all components of the $\mathbf{T}^{n,HSF}$ with an odd number

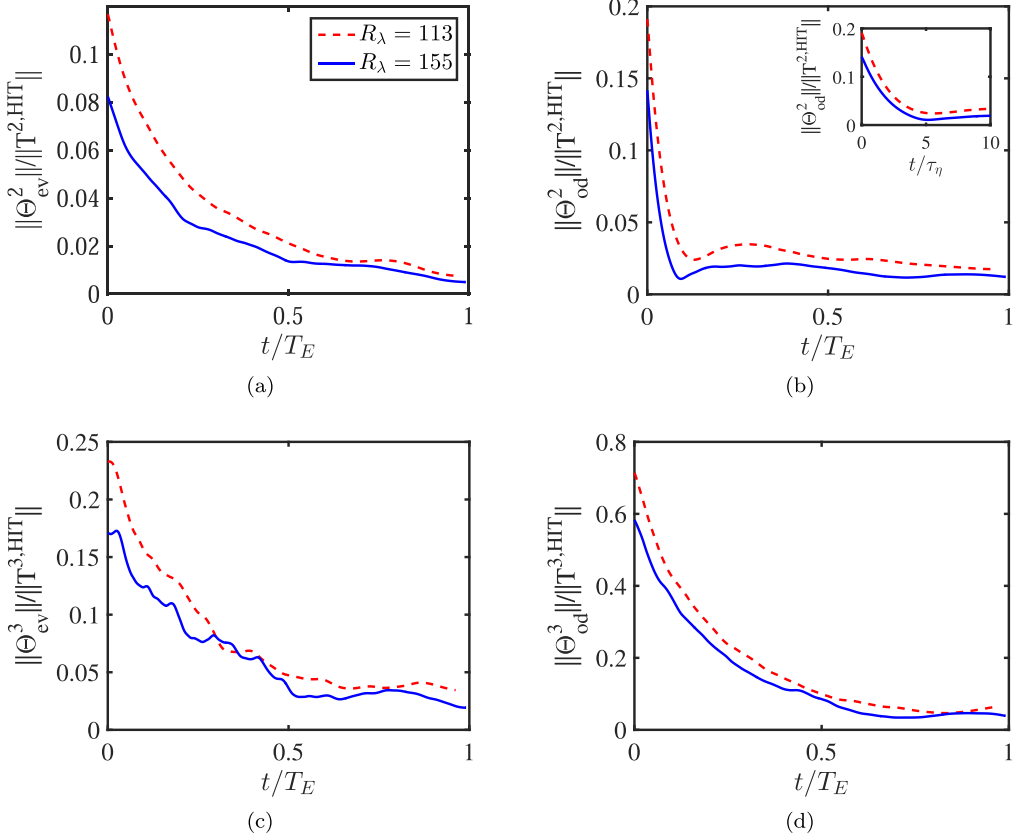


FIG. 5. Evolution of norms of odd and even parts of deviation $\Theta_{od,ev}^n$ normalized by $\|\mathbf{T}^{n,HIT}\|$ ($n = 2, 3$), (a) $\|\Theta_{ev}^2\|/\|\mathbf{T}^{2,HIT}\|$, (b) $\|\Theta_{od}^2\|/\|\mathbf{T}^{2,HIT}\|$, (c) $\|\Theta_{ev}^3\|/\|\mathbf{T}^{3,HIT}\|$, and (d) $\|\Theta_{od}^3\|/\|\mathbf{T}^{3,HIT}\|$. Time has been scaled on all graphs by T_E , except in the inset of panel (b), where it was scaled by τ_η .

of 3 are zero. However, components of $\mathbf{T}^{n,HSF}$ with an odd number of 1 and 2 may be nonzero. We therefore write

$$\Theta^{n,flow} = \Theta_{od}^{n,flow} + \Theta_{ev}^{n,flow}, \quad (17)$$

where the components of $\Theta_{od}^{n,flow}$ ($\Theta_{ev}^{n,flow}$) are nonzero only when the number of 1 and 2 are odd (even). Combining Eqs. (16) and (17) allows us to estimate the deviation with respect to isotropy, by separating the contributions. In the following, we will drop the “flow” superscript, as we are restricting ourselves to the homogeneous shear-released turbulence only.

We also notice that the diagonal components of \mathbf{b}^ω always involve an even number of any of the three spatial indices. In comparison, the off-diagonal terms involve an odd number of some indices. Similar to the HSF case, terms with an odd numbers of 3 are automatically 0, but terms with an odd number of indices 1 or 2 may be nonzero.

Figure 5 shows the temporal evolution of the norms of the even and odd components of $\Theta^{2,3}$. Namely, Θ_{ev}^2 decreases slowly towards 0, with a long timescale, of the order of T_E . In comparison, Θ_{od}^2 decays first very quickly, in a time of the order of a few τ_η . The further relaxation occurs over a longer timescale. The odd components of the third moment, Θ_{od}^3 , also decays slowly, possibly over a timescale of order T_E . We stress that the size of $\|\Theta_{od}^3\|$ is, in the dimensionless form chosen, $\gtrsim 0.5$, so the large anisotropy imprinted on the velocity gradient by the shear in the steady state remains

significant for a long time, of the order T_E . Similarly, we observe that the comparatively smaller even component of Θ_{ev}^3 also decays rather slowly, with a timescale of order T_E over the range of Reynolds number studied here. The behavior of $\Theta^{2,3}$ generally corroborates the observations in Fig. 3 and Fig. 4. We recall that the diagonal components of \mathbf{b}^ω contribute to the even components of Θ^2 . The off-diagonal term b_{12}^ω as well as the skewness $S_{\partial_2 u_1}$ and S_{ω_3} contribute to the odd components of Θ^2 and Θ^3 .

To summarize, we find that, aside from the odd components of Θ^2 , which exhibits a very fast decay, over a timescale of a few τ_η , followed by a slower decay, over a longer timescale, the even component of Θ^2 , as well as the third-order components, Θ^3 , all decay with a slower timescale. Our numerical results, however, do not allow us to clearly identify the characteristic timescales of the decay. In the following section, we consider the initial decay rates at $t = 0^+$ with the help of a theoretical analysis of the equations.

C. Theoretical analysis

In this subsection, we analyze the evolution of the tensor \mathbf{b}^ω by taking advantage of the absence of the pressure term in the equation for vorticity.

Returning to the definition, Eq. (12), we obtain the equation of evolution for \mathbf{b}^ω :

$$\frac{db_{ij}^\omega}{dt} = \frac{1}{\langle \omega^2 \rangle} \left[\frac{d\langle \omega_i \omega_j \rangle}{dt} - \chi \left(\frac{1}{3} \delta_{ij} + b_{ij}^\omega \right) \right] \quad \text{with} \quad \chi \equiv \frac{d\langle \omega^2 \rangle}{dt}. \quad (18)$$

To estimate the various terms in Eq. (18), we use the Navier-Stokes equations for the components of the velocity fluctuations in the presence of the external shear:

$$\frac{\partial}{\partial t} u_k + Sx_2 \partial_1 u_k + S\delta_{k1} u_2 + u_l \partial_l u_k = \nu \nabla^2 u_k - \frac{1}{\rho} \partial_k p', \quad (19)$$

which leads to the following equations for the partial derivatives of the velocity, $\partial_j u_k$:

$$\left(\frac{\partial}{\partial t} + Sx_2 \partial_1 + u_l \partial_l \right) \partial_j u_k + S\delta_{k1} \partial_j u_2 + S\delta_{j2} \partial_1 u_k + (\partial_j u_l \partial_l u_k) = \nu \nabla^2 (\partial_j u_k) - \frac{1}{\rho} \partial_{jk}^2 p'. \quad (20)$$

The equation for the vorticity can be readily obtained by using the identity $\omega_i = \epsilon_{ijk} \partial_j u_k$. Separating the three components of the vorticity, one obtains

$$\frac{D\omega_1}{Dt} = -S\partial_1 u_3 + \omega_k \partial_k u_1 + \nu \nabla^2 \omega_1, \quad (21)$$

$$\frac{D\omega_2}{Dt} = -S\partial_3 u_2 + \omega_k \partial_k u_2 + \nu \nabla^2 \omega_2, \quad (22)$$

$$\frac{D\omega_3}{Dt} = -S\partial_3 u_3 + \omega_k \partial_k u_3 + \nu \nabla^2 \omega_3, \quad (23)$$

where we have introduced the (Lagrangian) time derivative operator $\frac{D}{Dt} \equiv \partial_t + Sx_2 \partial_1 + u_l \partial_l$.

The equations for the second moments of ω_i can be readily deduced from Eqs. (21)–(23). We show below the results for $\langle \omega_1 \omega_1 \rangle$ and $\langle \omega_1 \omega_2 \rangle$, the results for $\langle \omega_2 \omega_2 \rangle$ and $\langle \omega_3 \omega_3 \rangle$ being similar:

$$\frac{1}{2} \frac{d}{dt} \langle \omega_1 \omega_1 \rangle = -S \langle \omega_1 \partial_1 u_3 \rangle + \langle \omega_1 \omega_k \partial_k u_1 \rangle + \nu \langle \omega_1 \nabla^2 \omega_1 \rangle, \quad (24)$$

$$\frac{d}{dt} \langle \omega_1 \omega_2 \rangle = -S \langle \omega_1 \partial_3 u_2 + \omega_2 \partial_1 u_3 \rangle + \langle \omega_k (\omega_1 \partial_k u_2 + \omega_2 \partial_k u_1) \rangle + \nu \langle \omega_2 \nabla^2 \omega_1 + \omega_1 \nabla^2 \omega_2 \rangle. \quad (25)$$

In the statistically steady state, the time derivatives on the left-hand side of Eqs. (24) and (25) are all identically zero, which imposes that the terms on the r.h.s. of the equations sum up to 0. More specifically, the first term that contains the shear rate S is balanced by the sum of the other two terms on the r.h.s. When the shear is released at $t = 0$, the first term vanishes but the values of all other

terms remain the same at $t = 0^+$. Therefore, the time derivatives of the moments at $t = 0^+$ simply become

$$\frac{d}{dt} \langle \omega_1 \omega_1 \rangle \Big|_{t=0^+} = 2 \left(\langle \omega_1 \omega_k \partial_k u_1 \rangle \Big|_{t=0} + \nu \langle \omega_1 \nabla^2 \omega_1 \rangle \Big|_{t=0} \right) = +2S \langle \omega_1 \partial_1 u_3 \rangle \Big|_{t=0^-} \quad (26)$$

and, similarly, for $\langle \omega_1 \omega_2 \rangle$ and $\chi(0^+)$:

$$\frac{d}{dt} \langle \omega_1 \omega_2 \rangle \Big|_{t=0^+} = +S \langle \omega_1 \partial_3 u_2 + \omega_2 \partial_1 u_3 \rangle \Big|_{t=0^-}, \quad (27)$$

$$\chi(0^+) = 2S \langle \omega_1 \partial_1 u_3 + \omega_2 \partial_2 u_3 + \omega_3 \partial_3 u_3 \rangle. \quad (28)$$

This, in turn, leads to the following equations for b_{11}^ω and b_{12}^ω :

$$\frac{db_{11}^\omega}{dt} \Big|_{t=0^+} = \frac{1}{\langle \omega^2 \rangle} \left\{ 2S \langle \omega_1 \partial_1 u_3 \rangle - \chi(0^+) \times \left[\frac{1}{3} + b_{11}^\omega(0) \right] \right\}, \quad (29)$$

$$\frac{db_{12}^\omega}{dt} \Big|_{t=0^+} = \frac{1}{\langle \omega^2 \rangle} \left[S \langle \omega_1 \partial_3 u_2 + \omega_2 \partial_1 u_3 \rangle - \chi(0^+) \times b_{12}^\omega(0) \right]. \quad (30)$$

We analyze first the evolution of b_{12}^ω . For the present discussion, it is important to notice that the terms on the r.h.s. of Eq. (30) involve only terms of the form $\langle \partial_a u_b \partial_c u_d \rangle$ with an even number of index 1, 2, or 3, which are nonzero even in the case of HIT flows, for which

$$\langle \omega_1 \partial_3 u_2 \rangle = \langle \omega_2 \partial_1 u_3 \rangle = -\langle (\partial_3 u_2)^2 \rangle = -\frac{2\varepsilon}{15\nu} \sim -\tau_\eta^{-2}. \quad (31)$$

This provides a very good estimate for $\frac{d}{dt} \langle \omega_1 \omega_2 \rangle$ at $t = 0^+$, since the deviation of the tensor $\langle \partial_a u_b \partial_c u_d \rangle$ from its HIT value, with the same dissipation and viscosity, is small. Furthermore, the expression for $\chi(0^+)$, Eq. (28), involves terms of the form $\langle \partial_a u_b \partial_c u_d \rangle$ with an even number of indices 3, but an odd number of indices 1 or 2. According to the arguments of Corrsin [39] and Lumley [40], these terms can be estimated as

$$\langle \omega_1 \partial_1 u_3 \rangle \sim \langle \omega_2 \partial_2 u_3 \rangle \sim \langle \omega_3 \partial_3 u_3 \rangle \sim S/\tau_\eta, \quad (32)$$

so $\chi(0^+) \sim S^2/\tau_\eta$.

Last, $\langle \omega_1 \omega_2 \rangle$ itself is a combination of terms of the form $\langle \partial_a u_b \partial_c u_d \rangle$, with an even number of index 3 but an odd number of index 1 or 2, so according to the arguments already used [39,40]:

$$\langle \omega_1 \omega_2 \rangle \sim \langle \omega^2 \rangle \times (S\tau_\eta) \sim S/\tau_\eta \quad \text{and} \quad b_{12}^\omega \sim S\tau_\eta, \quad (33)$$

which justifies that the magnitude of b_{12}^ω is in fact small and decreasing with the Reynolds number, consistent with the observations of Fig. 3. In addition, where $S\tau_\eta \ll 1$, the consequence of these estimates is that the term $\chi(0^+) b_{12}^\omega$ is subdominant in the r.h.s. of Eq. (30), which is of order $db_{12}^\omega/dt|_{t=0^+} \sim S$. Balancing the various terms in Eq. (30) therefore imposes that at $t = 0^+$, the timescale of the dynamics of b_{12}^ω is of order τ_η . This conclusion is consistent with the observation in Fig. 3 that $b_{12}^\omega = \langle \omega_1 \omega_2 \rangle / \langle \omega^2 \rangle$ evolves fast, over a characteristic timescale τ_η .

Turning now to the diagonal component b_{11}^ω , we observe that the terms on the r.h.s. of Eq. (29) involve only terms with an odd number of 1 and 2, and an even number of 3, which can be estimated according to Eq. (32). Taking into account the weak value of $b_{11}^\omega(0) \ll \frac{1}{3}$, we conclude that the r.h.s. of Eq. (29) is of the order $db_{11}^\omega/dt|_{t=0^+} \sim S^2\tau_\eta$. The magnitude of b_{11}^ω itself, which is zero for HIT, is similarly estimated by using

$$\left(\langle \omega_i^2 \rangle - \langle \omega^2 \rangle / 3 \right) \sim S/\tau_\eta, \quad (34)$$

which leads to an estimate of the initial values of the diagonal terms as $b_{ii}^\omega(0) \sim (S/\tau_\eta) / \langle \omega^2 \rangle \sim S\tau_\eta$. According to these estimates, all nonzero components of $b_{ij}^\omega(0)$ are of the order of $S\tau_\eta \ll 1$. Together, the estimates for $b_{11}^\omega(0)$ and $db_{11}^\omega/dt|_{t=0^+}$ lead to the conclusion that b_{11}^ω evolves with

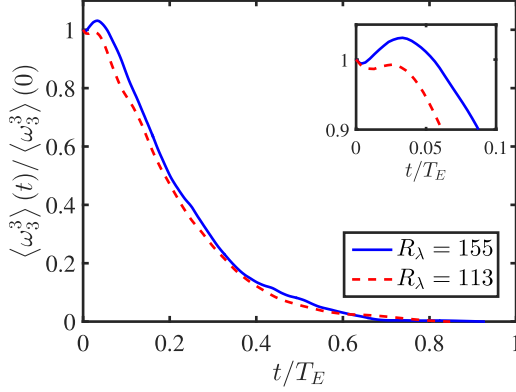


FIG. 6. Evolution of the normalized third moment of the spanwise component of vorticity, ω_3 . The relaxation of this moment occurs over a timescale of the order T_E , as predicted by the elementary considerations developed in this text. As shown in the inset, however, the evolution of the third moment is nonmonotonic. The full lines correspond to $R_\lambda = 155$ and the dashed lines to $R_\lambda = 113$.

a characteristic timescale of S^{-1} . It is straightforward to generalize these estimates to the other diagonal components of \mathbf{b}^ω . The conclusion of this analysis is therefore that the diagonal terms of \mathbf{b}^ω evolve much more slowly than b_{12}^ω .

While the Corrsin and Lumley argument [39,40] is plausible, given known measurements [37], deviations from this simple prediction have been reported, in particular for the third moment of $\partial_2 u_1$ in a turbulent shear flow [23]. Although the range of Reynolds numbers in numerical simulations is rather limited, and therefore does not allow us to reach an unambiguous conclusion regarding the magnitude of the deviations from isotropy, it was observed [42] that the even and odd components of the second-order tensor $\langle \partial_a u_b \partial_c u_d \rangle$ may actually decay differently with the Reynolds number, possibly with two different power laws: $\propto \langle \omega^2 \rangle (S/\tau_\eta) (S\tau_\eta)^{\alpha_{ev,od}^2}$, where the exponents α_{od}^2 and α_{ev}^2 describe the rate of decay of the odd and even components, respectively. An elementary order of magnitude analysis then leads to the prediction that the diagonal components b_{ii}^ω decay over a characteristic timescale of the order $S^{-1} (S\tau_\eta)^{\alpha_{ev}^2 - \alpha_{od}^2}$. The values provided in Ref. [42] are $\alpha_{ev}^2 \approx 1$ and $\alpha_{od}^2 \approx 1/2$, which implies that the characteristic timescale is of order $(S^{-1} \tau_\eta)^{1/2}$, i.e., half way between τ_η and T_E . We note that data from our two runs with $R_\lambda = 113$ and 155 indeed suggest that $(S^{-1} \tau_\eta)^{1/2}$ describes better the decay process of b_{ii}^ω . The range of the Reynolds number in our study, however, is not sufficient to unambiguously distinguish whether the timescale is $(S^{-1} \tau_\eta)^{1/2}$ or T_E .

The analysis presented here for $\langle \omega_3 \omega_3 \rangle$ can be easily extended to the third moment $\langle \omega_3 \omega_3 \omega_3 \rangle$:

$$\left. \frac{d}{dt} \langle \omega_3^3 \rangle \right|_{t=0^+} = +3S \langle \omega_3^2 \partial_3 u_3 \rangle. \quad (35)$$

As it was the case for $\langle \omega_3 \omega_3 \rangle$, a straightforward application of the timescale analysis, taking into account possible deviations from the Corrsin-Lumley argument [39,40], leads to the prediction that the characteristic timescale of relaxation of $\langle \omega_3^3 \rangle$ is $\sim S^{-1}$, possibly up to corrections in the form of powers of $\sim (S\tau_\eta)^{\alpha_{ev}^3 - \alpha_{od}^3}$, where α_{od}^3 and α_{ev}^3 describe the dependence on R_λ of the odd and even deviations of the tensors $\mathbf{T}^{3,HSF}$ from the isotropic case.

We notice that Eq. (35) predicts that at $t = 0^+$, $\frac{d}{dt} \langle \omega_3^3 \rangle > 0$. Since the initial steady-state value of $\langle \omega_3^3 \rangle$ is negative, this inequality does predict that the third moment $\langle \omega_3^3 \rangle$ decays towards the isotropic value of 0, as expected. The actual time dependence of $\langle \omega_3^3 \rangle$, however, is nonmonotonic. As shown in Fig. 6, in particular the inset, $\langle \omega_3^3 \rangle / \langle \omega_3^3 \rangle(0)$ first decays for a very short time, and then increases, before decreasing and relaxing towards zero at long times. The validity of the approximation $\langle \omega_3^3 \rangle(t) \approx \langle \omega_3^3 \rangle(0) + 3S \langle \omega_3^2 \partial_3 u_3 \rangle \times t$, therefore turns out to be rather limited: the

first-order approximation at $t = 0^+$ is clearly insufficient to unambiguously predict the evolution at longer times. Nonetheless, despite this obvious shortcoming, the considerations developed here lead to a simple estimate of the timescales involved, compatible with our own numerical data.

The observation that the moments of quantities that characterize the small-scale properties of the flow decay with a timescale that is much longer than the Kolmogorov scale points to a subtle relation between the temporal and spatial scales of motion. As observed in Sec. III, the pressure-rate-of-strain correlation, R_{ij} , can be expressed in an elementary manner in terms of the third moments of the velocity derivative correlations, Eq. (11). A fast decay, over a timescale τ_η of the third-order correlation tensor of $\partial_a u_b$, would have been difficult to combine with the slow decay of R_{ij} , and ultimately with that of the Reynolds stress tensor. We note that this observed slow decay of the anisotropy of the small scales in the shear-released flow resembles the slow change of the energy dissipation rate in a freely decaying HIT. While the two problems might be governed by different dynamics, they share one common feature that the small-scale quantity is tied to large-scale dynamics by averaged balance equations: $dk/dt = -\varepsilon$ and Eq. (11), respectively.

V. DISCUSSION AND CONCLUSIONS

We have investigated the return to isotropy of a homogeneous turbulent flow, initially in the presence of a large-scale uniform shear and in statistical steady state, after the imposed shear is released. Our investigation complements other studies, considering the return towards isotropy of turbulent flows with different imposed mean gradients [12].

From a fundamental point of view, one of the main motivations of this work was to understand how the anisotropy of the flow, present at all scales, relaxes when the source of anisotropy is removed. Previous studies show that in the case of a shear flow, the small scales are anisotropic and that anisotropy decreases with the increase of the Reynolds number, although slower than that expected from elementary considerations based on the Kolmogorov theory. For example, experimental data indicate that the value of the skewness of $\partial_2 u_1$ decays as $\sim R_\lambda^{-1/2}$, slower than the expected scaling of R_λ^{-1} , and is still $O(1)$ at $R_\lambda \approx 100$ [23]. In this work, we investigated two flows at $R_\lambda = 113$ and 155, respectively, in which the small-scale anisotropy is significant. We focused specifically on the anisotropy present at the largest scales, measured by the Reynolds stress tensor, as well as at the smallest scales, measured by the moments of the velocity gradient tensor, $\langle \partial_a u_b \partial_c u_d \rangle$ or $\langle \partial_a u_b \partial_c u_d \partial_e u_f \rangle$.

Our results show that the return to isotropy of the Reynolds stress tensor in the homogeneous shear-released turbulence is qualitatively similar to what has been observed in other flows [12,36], albeit with some minor difference in the rate of return to isotropy, compared to the rate of decay of the kinetic energy.

One of the major results of this work is that the decay of the anisotropy present at the smallest scales, characterized in particular by the second moment of the vorticity tensor, \mathbf{b}^ω [see Eq. (12)], involves more than one timescale. Whereas the off-diagonal term, b_{12}^ω decays first very fast, with a characteristic timescale $\sim \tau_\eta$, the diagonal terms b_{ii}^ω decay over a much longer timescale. Our simplified analysis, using the Corrsin-Lumley estimate for the small-scale anisotropy [39,40], suggests a timescale of the order S^{-1} , i.e., the timescale associated with the large scales of the flow. The deviations due to the dependence on R_λ of the odd and even components of the moments of the velocity gradient tensor [42] could suggest a different timescale, $\sim (S^{-1} \tau_\eta)^{1/2}$. The limited range of values of R_λ covered by our simulations, however, does not allow us to unambiguously distinguish the two.

The elementary theoretical arguments used above can also explain why the skewness of the spanwise component of the vorticity, ω_3 , also decays very slowly. Thus, the relatively large anisotropy at small scales, such as ω_3 , or equivalently, the normal derivative of the streamwise velocity component, persists over a long time. A straightforward extension of the analysis presented in Sec. IV C also makes it clear that the relaxation towards isotropy depend on the specific properties of the flow.

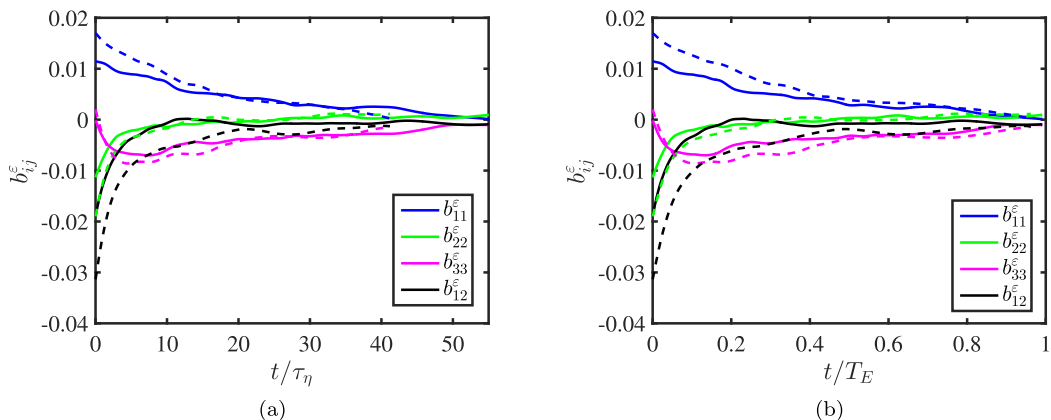


FIG. 7. Evolution of the components of the dissipation anisotropy tensor b_{ij}^{ϵ} , defined by Eq. (7), as a function of t/τ_{η} (a); and as a function of t/T_E , (b). Full lines correspond to the solution at $R_{\lambda} = 155$ and dashed lines to $R_{\lambda} = 113$.

The possibility that quantities measuring the anisotropy at small scales, based on the velocity gradient tensors, decay over a long timescale, compared to τ_{η} , is clearly of theoretical interest. We notice in this respect that the relation between the pressure-rate-of-strain correlation tensor R_{ij} [see Eq. (8)] responsible for the return to isotropy of the large scale, and the third-order correlation $\langle \partial_a u_b \partial_c u_d \partial_e u_f \rangle$, through Eq. (11), was making it in fact rather implausible that the former would relax rapidly to isotropy whereas the latter would relax over a much longer timescale. To conclude, the present study demonstrates that the separation between the timescales characterizing the return to isotropy at large and small scales does not reduce to a straightforward extension of Kolmogorov phenomenology. A proper understanding and modeling of these effects requires further investigation.

ACKNOWLEDGMENTS

P.F.Y. and H.X. are grateful for the financial support from the National Natural Science Foundation of China under grant number 11672157. A.P. gratefully acknowledges the support from the IDEXLyon project (Contract no. ANR-16-IDEX-0005) under University of Lyon auspices and from ANR project TILT (Contract no. ANR-20-CE30-0035).

APPENDIX A: RETURN OF THE TENSOR ε_{ij} TO ISOTROPY

We briefly consider in this Appendix the return to isotropy of the dissipation tensor, defined by Eq. (7), which plays a role in the return to equilibrium of the anisotropy tensor \mathbf{b} via Eq. (6). To that end, we consider the anisotropy tensor defined as $b_{ij}^{\epsilon} \equiv \frac{\varepsilon_{ij}}{2\varepsilon} - \frac{1}{3}\delta_{ij}$. This tensor provides an alternative way to describe the relaxation of small-scale quantities when the shear is released.

Figure 7 shows how the components of b_{ij}^{ϵ} change with time, both as a function of τ/τ_{η} and as a function of τ/T_E for the two Reynolds numbers, where the timescales τ_{η} , the Kolmogorov timescale, and T_E , the integral timescales, are defined by Eq. (2), as explained in Sec. II B. Comparison of Figs. 7(a) and 7(b) suggests that overall, the anisotropy of ε_{ij} actually decays over a timescale given by T_E , rather than by the Kolmogorov time. Interestingly, the magnitude of the component b_{33}^{ϵ} increases rapidly, over a timescale of order τ_{η} , before it finally decays gradually towards zero over a timescale of order T_E , which is different from other components. This suggests that the dynamics of small-scale quantities are controlled by mechanisms involving more than one timescale, depending on the components of the tensor.

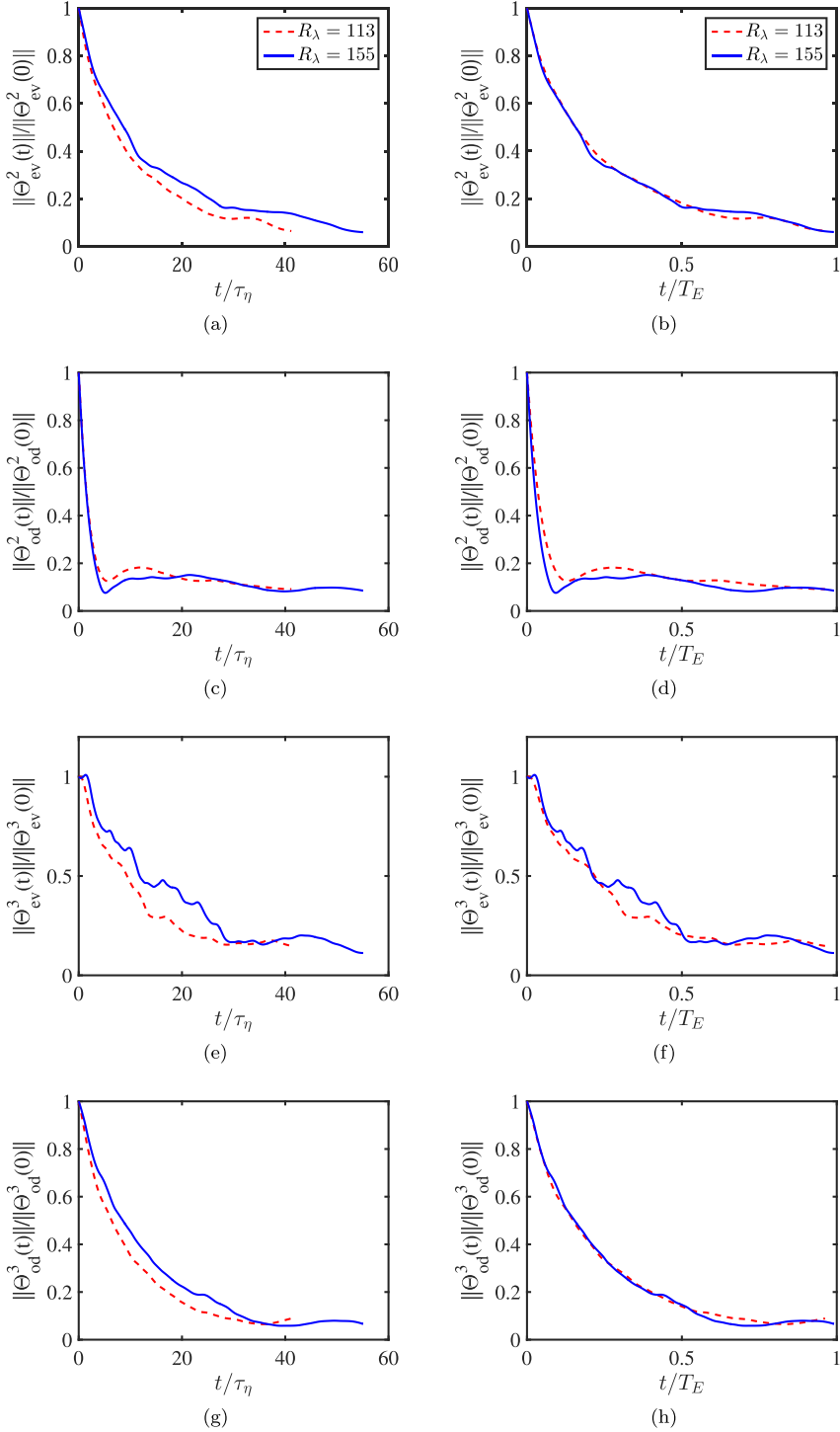


FIG. 8. Evolution of norms of odd and even parts of deviation $\Theta_{od,ev}^n$ normalized by its values at $t = 0$. $\|\Theta_{ev}^2\|(t)/\|\Theta_{ev}^2\|(0)$, time t normalized by (a) τ_η and (b) T_E , $\|\Theta_{od}^2\|(t)/\|\Theta_{od}^2\|(0)$, time t normalized by (c) τ_η , and (d) T_E , $\|\Theta_{ev}^3\|(t)/\|\Theta_{ev}^3\|(0)$, time t normalized by (e) τ_η and (f) T_E , $\|\Theta_{od}^3\|(t)/\|\Theta_{od}^3\|(0)$, time t normalized by (g) τ_η and (h) T_E .

APPENDIX B: TIME EVOLUTION OF $\Theta_{od,ev}^n$ NORMALIZED BY T_E AND τ_η

In this Appendix we show in Fig. 8 the quantities shown in Fig. 5 in a different way, where we use the value at $t = 0$ instead of $\|\mathbf{T}^{n,HIT}\|$ to normalize $\|\Theta_{od,ev}^n\|$. In addition, for every quantity of $\|\Theta_{od,ev}^n\|$ ($n = 2, 3$), we show the time normalization for both T_E and τ_η . As a result, curves in every panel of Fig. 8 start from unity, and this helps us to evaluate which timescale collapses those curves better. One could readily see that T_E works better for $\|\Theta_{ev}^2\|$ and $\|\Theta_{od,ev}^3\|$, while τ_η is the better choice for $\|\Theta_{od}^2\|$.

-
- [1] U. Frisch, *Turbulence: The Legacy of A. N. Kolmogorov* (Cambridge University Press, Cambridge, 1995).
 - [2] T. Ishihara, Y. Kaneda, M. Yokokawa, K. Itakura, and A. Uno, Small-scale statistics in high-resolution direct numerical simulation of turbulence: Reynolds number dependence of one-point velocity gradient statistics, *J. Fluid Mech.* **592**, 335 (2007).
 - [3] T. Ishihara, K. Morishita, M. Yokokawa, A. Uno, and Y. Kaneda, Energy spectrum in high-resolution direct numerical simulations of turbulence, *Phys. Rev. Fluids* **1**, 082403(R) (2016).
 - [4] D. Buaria, A. Pumir, and E. Bodenschatz, Self-attenuation of extreme events in Navier-Stokes turbulence, *Nat. Commun.* **11**, 5852 (2020).
 - [5] M. Sinhuber, E. Bodenschatz, and G. P. Bewley, Decay of Turbulence at High Reynolds Numbers, *Phys. Rev. Lett.* **114**, 034501 (2015).
 - [6] C. Küchler, G. Bewley, and E. Bodenschatz, Experimental study of the bottleneck in fully developed turbulence, *J. Stat. Phys.* **175**, 617 (2019).
 - [7] H. Tennekes and J. L. Lumley, *A First Course in Turbulence* (MIT Press, Cambridge, MA, 1972).
 - [8] S. B. Pope, *Turbulent Flows* (Cambridge University Press, Cambridge, 2000).
 - [9] S. Ayyalasomayajula and Z. Warhaft, Nonlinear interactions in strained axisymmetric high-Reynolds-number turbulence, *J. Fluid Mech.* **566**, 273 (2006).
 - [10] J. Chen, C. Meneveau, and J. Katz, Scale interactions of turbulence subjected to a straining-relaxation-destraining cycle, *J. Fluid Mech.* **562**, 123 (2006).
 - [11] P. Gualtieri and C. Meneveau, Direct numerical simulations of turbulence subjected to a straining and destraining cycle, *Phys. Fluids* **22**, 065104 (2010).
 - [12] M. P. Clay and P.-K. Yeung, A numerical study of turbulence under temporally evolving axisymmetric contraction and subsequent relaxation, *J. Fluid Mech.* **805**, 460 (2016).
 - [13] F. H. Champagne, V. G. Harris, and S. Corrsin, Experiments on nearly homogeneous turbulent shear flow, *J. Fluid Mech.* **41**, 81 (1970).
 - [14] V. G. Harris, J. A. H. Graham, and S. Corrsin, Further experiments in nearly homogeneous turbulent shear flow, *J. Fluid Mech.* **81**, 657 (1977).
 - [15] S. Tavoularis and S. Corrsin, Experiments in nearly homogeneous shear flow with a uniform mean temperature gradient. Part 1. *J. Fluid Mech.* **104**, 311 (1981).
 - [16] M. M. Rogers and P. Moin, The structure of the vorticity field in homogeneous turbulent flows, *J. Fluid Mech.* **176**, 33 (1987).
 - [17] M. J. Lee, J. Kim, and P. Moin, Structure of turbulence at high shear rate, *J. Fluid Mech.* **216**, 561 (1990).
 - [18] S. Kida and M. Tanaka, Dynamics of vortical structures in a homogeneous shear flow, *J. Fluid Mech.* **274**, 43 (1994).
 - [19] A. Briard, T. Gomez, V. Mons, and P. Sagaut, Decay and growth laws in homogeneous shear turbulence, *J. Turbul.* **17**, 699 (2016).
 - [20] A. Pumir and B. I. Shraiman, Persistent Small Scale Anisotropy in Homogeneous Shear Flows, *Phys. Rev. Lett.* **75**, 3114 (1995).
 - [21] A. Pumir, Turbulence in homogeneous shear flows, *Phys. Fluids* **8**, 3112 (1996).
 - [22] S. Garg and Z. Warhaft, On the small scales of simple shear flows, *Phys. Fluids* **10**, 662 (1998).
 - [23] X. Shen and Z. Warhaft, The anisotropy of the small scale structure in high Reynolds number ($R_\lambda \sim 1000$) turbulent shear flow, *Phys. Fluids* **12**, 2976 (2000).

- [24] J. Schumacher and B. Eckhardt, On statistically stationary homogeneous shear turbulence, *Europhys. Lett.* **52**, 627 (2000).
- [25] L. Biferale and M. Vergassola, Isotropy vs anisotropy in small-scale turbulence, *Phys. Fluids* **13**, 2139 (2001).
- [26] P. Gualtieri, C. M. Casciola, R. Benzi, G. Amati, and R. Piva, Scaling laws and intermittency in homogeneous shear flow, *Phys. Fluids* **14**, 583 (2002).
- [27] C. M. Casciola, P. Gualtieri, B. Jacob, and R. Piva, The residual anisotropy at small scales in high shear turbulence, *Phys. Fluids* **19**, 101704 (2007).
- [28] J. C. Isaza and L. R. Collins, Effect of the shear parameter on velocity-gradient statistics in homogeneous turbulent shear flow, *J. Fluid Mech.* **678**, 14 (2011).
- [29] J. I. Cardesa, A. Vela-Martin, S. Dong, and Javier Jiménez, The temporal evolution of the energy flux across scales in homogeneous turbulence, *Phys. Fluids* **27**, 111702 (2015).
- [30] A. Sekimoto, S. Dong, and J. Jiménez, Direct numerical simulation of statistically stationary and homogeneous shear turbulence and its relation to other shear flows, *Phys. Fluids* **28**, 035101 (2016).
- [31] S. Dong, A. Lozano-Durín, A. Sekimoto, and J. Jiménez, Coherent structures in statistically stationary homogeneous shear turbulence, *J. Fluid Mech.* **816**, 167 (2017).
- [32] A. Pumir, H. Xu, and E. D. Siggia, Small-scale anisotropy in turbulent boundary layers, *J. Fluid Mech.* **804**, 5 (2016).
- [33] T.-H. Shih and J. L. Lumley, Critical comparison of second-order closures with direct numerical simulations of homogeneous turbulence, *AIAA J.* **31**, 663 (1993).
- [34] J. Rotta, Statistische Theorie nichthomogener Turbulenz, *Z. Phys.* **129**, 547 (1951).
- [35] J. L. Lumley and G. R. Newman, The return to isotropy of homogeneous turbulence, *J. Fluid Mech.* **82**, 161 (1977).
- [36] K. S. Choi and J. L. Lumley, The return to isotropy of homogeneous turbulence, *J. Fluid Mech.* **436**, 59 (2001).
- [37] S. G. Saddoughi and S. V. Veeravalli, Local isotropy in turbulent boundary layers at high Reynolds numbers, *J. Fluid Mech.* **268**, 333 (1994).
- [38] H. E. Cekli and W. van de Water, Stirring anisotropic turbulence with an active grid, *Phys. Fluids* **32**, 075119 (2020).
- [39] S. Corrsin, Local isotropy in turbulent shear flow, NACA Res. Memo 58B11 (1958).
- [40] J. L. Lumley, Similarity and the turbulent energy spectrum, *Phys. Fluids* **10**, 855 (1967).
- [41] R. S. Rogallo, Numerical experiments in homogeneous turbulence, NASA Tech. Memo. 81315 (1981).
- [42] A. Pumir, Structure of the velocity gradient tensor in turbulent shear flows, *Phys. Rev. Fluids* **2**, 074602 (2017).
- [43] A. W. Vreman and J. G. M. Kuerten, Statistics of spatial derivatives of velocity and pressure in turbulent channel flow, *Phys. Fluids* **26**, 085103 (1991).
- [44] Y. Li, E. Perlman, M. Wan, Y. Yang, C. Meneveau, R. Burns, S. Chen, A. Szalay, and G. Eyink, A public turbulence database cluster and application to study Lagrangian evolution of velocity increments in turbulence, *J. Turbulence* **9**, 131 (2008).
- [45] A. Pumir, A numerical study of pressure fluctuations in three-dimensional, incompressible homogeneous isotropic turbulence, *Phys. Fluids* **6**, 2071 (1994).
- [46] C. J. Zusi and J. B. Perot, Simulation and modeling of turbulence subjected to a period of uniform plane strain, *Phys. Fluids* **25**, 110819 (2013).
- [47] C. J. Zusi and J. B. Perot, Simulation and modeling of turbulence subjected to a period of axisymmetric contraction or expansion, *Phys. Fluids* **26**, 115103 (2014).
- [48] J. L. Lumley, Computational modelling of turbulent flows, *Adv. Appl. Mech.* **18**, 123 (1979).
- [49] Y. Li, The evolution towards the rod-like axisymmetric structure for turbulent stress tensor, *Phys. Fluids* **27**, 085104 (2015).
- [50] C. G. Speziale, S. Sarkar, and T. B. Gatski, Modelling the pressure-strain correlation of turbulence: An invariant dynamical systems approach, *J. Fluid Mech.* **227**, 245 (1991).
- [51] P.-F. Yang, A. Pumir, and H. Xu, Generalized self-similar spectrum and the effect of large-scale in decaying homogeneous isotropic turbulence, *New J. Phys.* **20**, 103035 (2018).